ChemComm

HIGHLIGHT

View Article Online
View Journal | View Issue

Check for updates

Cite this: *Chem. Commun.*, 2025, **61**, 8969

Recent progress in the decomposition of ammonia as a potential hydrogen-carrier using green technologies

Seyed Majid Ghoreishian,[a] Mohammad Norouzi[b] and Jochen Lauterbach *[a]

To meet the global carbon neutrality target set by the United Nations, finding alternative and cost-effective energy sources has become prominent while enhancing energy conversion methods' efficiency. The versatile applications of hydrogen (H_2) as an energy vector have been highly valued over the past decades due to its significantly lower greenhouse gas emissions compared to conventional fossil fuels. However, challenges related to H_2 generation and storage for portable applications have increasingly called attention to ammonia (NH_3) decomposition as an effective method for on-site hydrogen production due to its high hydrogen content, high energy density, and affordability. This review highlights recent developments in green decomposition techniques for ammonia, including photocatalysis, electrocatalysis, non-thermal plasma, and other techniques, with a focus on the latest developments in new methods and materials (catalysts, electrodes, and sorbents) employed in these processes. Moreover, technical challenges and recommendations are discussed to assess the future potential of ammonia in the energy sector. The role of machine learning and artificial intelligence in ammonia decomposition is also emphasized, as these tools open up ways of simulating reaction mechanisms for the exploration of a new generation of high-performance catalysts and reducing trial-and-error approaches.

Received 2nd December 2024,
Accepted 3rd April 2025

DOI: 10.1039/d4cc06382a

rsc.li/chemcomm

Open Access Article. Published on 04 aprel 2025. Downloaded on 28.01.2026 06:48:11.
This article is licensed under a Creative Commons Attribution-NonCommercial 3.0 Unported Licence.

1. Introduction

The demand for global energy has increased due to a highly energy-intensive lifestyle and the continuing growth of the world's population.[1] Currently, approximately 733 million people globally lack access to electricity, while 2.4 billion people lack clean fuels and modern cooking technologies.[2] According to the Energy Institute Statistical Review of World Energy 2023, fossil fuels, coal, oil, and natural gas are still the main primary energy sources (82%).[3] There is a broad consensus that fossil fuel reserves, particularly oil, will be on the verge of depletion and in shortage by the end of this century.[4] Due to the continuous reliance on fossil fuels, a substantial amount of greenhouse gases (GHGs) such as CO_2, CO, SO_2, NO_x, and volatile organic compounds (methane (CH_4), benzene (C_6H_6), formaldehyde (CH_2O), and ethanol (C_2H_5OH)) have been emitted into Earth's atmosphere.[5–8] CO_2 is recognized as the primary driver of global warming, with approximately 80% originating from the combustion of fossil fuels within the industrial sector.[9] To respond to global climate change and meet the Paris Agreement's temperature control goals, there is a worldwide consensus on reducing greenhouse gas emissions toward net-zero carbon emissions.[9] In this context, China has set a target to reach "peak carbon" by 2030 and "carbon neutrality" by 2060.[10]

Renewable energy technologies, including solar and wind power, are increasingly achieving cost parity with conventional fossil fuel-based energy sources.[11] However, as these energy sources are intermittent and unevenly distributed across the globe, it is still complex to completely replace traditional energy.[12] Therefore, hydrogen (H_2) has attracted attention as a new energy source without pollution or CO_2 emissions.

Hydrogen, with the smallest relative molecular mass, has attracted significant interest as a secondary energy source due to its high gravimetric energy density ($\sim$33 kW h kg^{-1}), which is greater than that of gasoline and diesel, and its capacity for zero-emission output.[13,14] The U.S. Department of Energy (DOE) initially set hydrogen storage targets in 2009 for applications such as portable power, onboard light-duty vehicles, and material-handling equipment. The DOE set specific targets for on-board hydrogen storage: 0.030 kg H_2 L^{-1} and 4.5 wt % for volumetric and gravimetric storage capacities by 2020.[15] In addition, China is actively working to increase its production of carbon-neutral hydrogen (green hydrogen) to meet its carbon neutrality goals, which involves water splitting (eqn (1) and (2))

[a] *Department of Chemical Engineering, University of South Carolina, Columbia, SC 29208, USA. E-mail: lauteraj@cec.sc.edu*
[b] *School of Cancer Sciences, University of Glasgow, Glasgow, UK*

Open Access Article. Published on 04 aprel 2025. Downloaded on 28.01.2026 06:48:11.
This article is licensed under a Creative Commons Attribution-NonCommercial 3.0 Unported Licence.

to extract hydrogen using electricity generated from renewable sources such as wind and solar energies.[9,16] It is expected that till 2025, the specific system targets aim for 1.8 kW h kg^{-1} system (0.055 kg H_2 kg^{-1} system), 1.3 kW h L^{-1} system (0.040 kg H_2 L^{-1}), and \$9 per kW h storage system (\$300 per kg stored H_2 system).

In acidic solution

$$2H_2O \rightarrow O_2 + 4H^+ + 4e^- \quad E^0 = 1.23 \text{ V } \textit{vs.} \text{ NHE}$$

$$4H^+ + 4e^- \rightarrow 2H_2 \quad E^0 = 0.00 \text{ V } \textit{vs.} \text{ NHE}$$

$$2H_2O \rightarrow 2H_2 + 2O_2 \quad E^0 = 1.23 \text{ V } \textit{vs.} \text{ NHE}, \Delta G^0 = 237.2 \text{ kJ mol}^{-1} \quad (1)$$

In alkaline solution

$$4OH^- \rightarrow O_2 + 2H_2O + 4e^- \quad E^0 = 0.4 \text{ V } \textit{vs.} \text{ NHE}$$

$$4H_2O + 4e^- \rightarrow 2H_2 + 4OH^- \quad E^0 = -0.83 \text{ V } \textit{vs.} \text{ NHE}$$

$$2H_2O \rightarrow 2H_2 + 2O_2 \quad E^0 = 1.23 \text{ V } \textit{vs.} \text{ NHE}, \Delta G^0 = 237.2 \text{ kJ mol}^{-1} \quad (2)$$

Currently, hydrogen can be stored in carbon fiber tanks at high pressures (>35 MPa), achieving a gravimetric H_2 capacity of 0.025 kg H_2 kg^{-1} at 350 bar.[17] Hydrogen can only be liquefied at an extremely low temperature of −253 °C or pressures above 70 MPa that significantly increase the costs associated with the storage and transportation of H_2 energy.[9] Therefore, the transportation and storage of hydrogen remains a critical barrier, significantly impeding its industrial applications.[14]

One potential solution to address hydrogen transport issues involves the utilization of liquid or solid hydrogen energy carriers, from which H_2 is chemically extracted upon arrival. The selection of a hydrogen energy carrier focuses on environmental friendliness, efficiency, ease of handling and transport, and a high hydrogen mass and volume percentage. Given this, methanol and ammonia are frequently discussed as feasible carriers.[9]

Accordingly, ammonia (NH_3) possesses high H_2 content (17.8 wt%) and a large energy density (3000 W h kg^{-1}). It has greater volumetric hydrogen density than liquid H_2 (121 kg H_2 m^{-3}) and can be liquefied and stored at room temperature, facilitating its transportation and storage, particularly in the liquid phase, as NH_3 gas is liquefied under a pressure of 8.5 MPa at 20 °C.[18,19] Notably, hydrogen produced through ammonia decomposition typically contains fewer impurities compared to hydrogen derived from hydrocarbons (like methanol).[20]

Ammonia decomposition has been investigated since the 19th century.[18] In 1904, Perman and Atkinson reported that complete decomposition of ammonia is not achievable below 1100 °C. They also noted that the degree of decomposition depends significantly on the nature of the surface in contact with the ammonia, particularly the catalysts involved.[20] To date, various metals, alloys, and their compounds (such as oxides and nitrides) have been extensively studied as active catalysts for NH_3 decomposition. Given that ammonia decomposition is the exact reverse of industrial ammonia synthesis from N_2 and H_2, the microkinetic principle suggests that catalysts effective for NH_3 generation should, in theory, facilitate ammonia decomposition. However, the catalytic activity trends differ significantly between the two processes due to their opposing reaction pathways and targeted products.[21]

Prior to 1990, Fe-based catalysts attracted significant interest; however, in the past decade, research has increasingly shifted toward noble metal catalysts, with growing attention on metal nitrides, carbides, and alloys as active components for the decomposition reaction.[22] Various monometallic systems based on non-noble metals have been investigated for hydrogen production from ammonia. Over the last decade, the catalytic decomposition of NH_3 over catalysts such as platinum (Pt), palladium (Pd), ruthenium (Ru), and rhodium (Rh) has gained a lot of attention in substitution of iron.[18] While these metals show outstanding activities, their large-scale applications significantly increase the cost, which is a substantial drawback.[23] To tackle this issue, transition metal carbides (MoC_x, VC_x, WC_x, and FeC_x) and nitrides (MoN_x, VN_x, and WN_x), along with zirconium oxynitrides, have been studied. Amidst those, molybdenum nitride and tungsten carbide have received the most attention in ammonia decomposition studies. Notably, these catalysts are generally evaluated under conditions relevant not only to hydrogen production but also to gasification mixture clean-up.[24] For bimetallic catalysts, several studies have been explored, including Ni–Pt, Ni/Ru, Pd/Pt/Ru/La, and Fe–MO_x (M = Ce, Al, Si, Sr, and Zr). However, a key challenge for bimetallic catalysts remains the structural stability of these catalysts under reaction conditions, particularly concerning metal segregation. This could lead to increased energy consumption, creating potential obstacles for the decomposition of NH_3.[25] Given that enhanced metal interactions appear to contribute to higher catalytic activity, optimizing preparation methods and selecting appropriate metal salts could offer promising strategies for improving performance.[26]

Research has shown that alloying strategies can play a crucial role in facilitating the ammonia decomposition reaction to their monometallic counterparts by improving the catalytic performance of catalysts.[25,27] In this area, a broad range of alloy systems have been developed, including Co alloys with Ni,[28] Re[29] and Ce,[30] Ni alloys with Co, Fe, and Cu,[31] Ru–Ni,[32] Cu–Zn,[33] *etc.* These findings demonstrate that alloy-based catalysts could provide a more cost-effective alternative while preserving—or even exceeding—the catalytic efficiency of noble metals.[34] However, choosing the right elements and appropriate stoichiometric composition remains a significant challenge for NH_3 decomposition over alloyed catalysts to ensure both optimal activity and long-term stability.[35] Therefore, one of the most significant challenges in the preparation of hydrogen from ammonia decomposition is to customize an effective catalyst that is energy efficient, highly selective, scalable, and affordable, providing a stable rate of decomposition at low temperatures.[36]

Recent research studies have shifted their focus from noble metals-based catalysts to alternative transition metal (TM) and TM-free catalysts. Among these, alkali amides and imides, particularly lithium (Li)-based compounds such as $LiNH_2$ and Li_2NH, have demonstrated a significant reduction in activation barriers by stabilizing M–N bond intermediates. Theoretical studies further highlight the importance of surface disorder dynamics

 This journal is © The Royal Society of Chemistry 2025

Open Access Article. Published on 04 apríl 2025. Downloaded on 28.01.2026 06:48:11.
This article is licensed under a Creative Commons Attribution-NonCommercial 3.0 Unported Licence.

Table 1 The effective heterogeneous catalysts utilized for the decomposition of ammonia[18]

Catalyst	Temperature (°C)	Conversion (%)	TOF (s^{-1})	Ref.
$Ni/MgAl_2O_4$-LDH	600	88.7	2.18	38
Co/NC-600	500	80		39
$Ru/SmCeO_x$	400	74.9	25.81	40
35Co/BHA	500	87.2		41
2.5Ru/10C-rGO	400	96	75.4	42
$CoRe_{1.6}$	500	~90		29
K^+–Fe/C	470	20	~0.5	43
Ru/Al_2O_3	580		6.85	44
$20Co–10Ni/Y_2O_3$	550	71.2		45
Co-containing CNTs	700	~100		46
Ni-10/ATP	650	64.3		47
α-FeO_2O_3-50@$pSiO_2$	800	100		48
10%Co/MWCNTs	600		8.15	49
$Ru/La_{0.33}Ce_{0.67}$	450	91.9	11.4	50
Ni_5Co_5/SiO_2	550	76.8		28
5CMLa-5	550	82.7		51
1%K–Co/SiC	350	33.1	9.3	52
Pr–Ni/Al_2O_3	550	~90		53

in non-stoichiometric lithium amide compounds ($Li_{2-x}(NH_2)_x$-$(NH)_{1-x}$) for TM-free catalysis, suggesting mechanistic differences from TM-based systems. Similar to TM-free NH_3 synthesis catalysts, lithium amides/imides exhibit catalytic activity for ammonia decomposition both with and without transition metals. Notably, addition of TM to $LiNH_2$ enhances NH_3 conversion at 440 °C from 54% to 86%, in which the catalytic performance was also influenced by ammonia flow rates.[37] Table 1 provides a summary of the effective heterogeneous catalysts used for the thermal decomposition of ammonia.

From this perspective, significant progress has been made in recent years in developing alternative methods, with a focus on reducing reaction temperatures. This advancement aims to lower energy consumption while enhancing hydrogen production efficiency.[54] Electric currents, electron beams, microwaves, plasma, and solar energy are alternative approaches to provide new feasible solutions for ammonia decomposition reaction (Fig. 1).[55] Although numerous reviews have been published on the progress of ammonia decomposition, the literature has overlooked assessing the different approaches for green H_2 generation from NH_3 and the subsequent technical barriers to achieving a futuristic fuel and sustainable energy vector.

Hence, this review aims to summarize and analyze previously reported green ammonia cracking aspects, such as photocatalysis, electrocatalysis, plasma, and other approaches, as well as their mechanisms of catalytic activity. Furthermore, the influences of recent revolution in data science, artificial intelligence (AI), and machine learning (ML) on the discovery of novel catalysts for the NH_3-to-H_2 reaction are evaluated. Finally, based on the literature and our experience, the current challenges and future perspectives for achieving rapid commercialization of NH_3 decomposition and green H_2 production are discussed.

2. Photocatalysis

In recent decades, the study of photocatalytic ammonia decomposition technology has garnered significant attention due to their potential applications in energy production, driven by growing concerns over environmental impact and the increasing demand for energy amid dwindling nonrenewable fossil fuel resources.[19] The photocatalytic decomposition of NH_3 into N_2 and H_2 presents a viable approach, as it can be conducted at room temperature using recyclable catalysts and allows facile control of light exposure *via* a switch. Moreover, utilizing sunlight for ammonia decomposition represents an artificial photosynthetic reaction that proceeds under alkaline conditions.[56]

Fundamentally, photocatalysis involves a redox reaction that utilizes photo-generated electrons (e^-) and holes (h^+) in semiconductors. The overall process unfolds in three key stages. First, photons excite charge carriers, initiating the reaction. Next, these charges are separated and migrate across the photocatalytic surface. Finally, the photo-induced charge carriers drive catalytic reactions at the surface, facilitating water oxidation and reduction. These steps are elaborated in eqn (3)–(12).[57–62]

$$\text{Photocatalyst} + h\nu \rightarrow h^+ + e^- \quad (3)$$

$$O_2 + e^- \rightarrow {}^\bullet O_2^- \quad E^0 = -0.33 \text{ V } \textit{vs.} \text{ NHE} \quad (4)$$

$$H_2O_2 + e^- + H^+ \rightarrow {}^\bullet OH + H_2O \quad E^0 = 0.38 \text{ V } \textit{vs.} \text{ NHE} \quad (5)$$

$$O_2 + 2e^- + 2H^+ \rightarrow H_2O_2 \quad E^0 = 0.68 \text{ V } \textit{vs.} \text{ NHE} \quad (6)$$

$$HO_2^- + H_2O + 2e^- \rightarrow 3OH^- \quad E^0 = 0.87 \text{ V } \textit{vs.} \text{ NHE} \quad (7)$$

$$2{}^\bullet O_2^- + 2H^+ + e^- \rightarrow H_2O_2 \quad E^0 = 0.89 \text{ V } \textit{vs.} \text{ NHE} \quad (8)$$

$${}^\bullet O_2H + H^+ + e^- \rightarrow H_2O_2 \quad E^0 = 1.49 \text{ V } \textit{vs.} \text{ NHE} \quad (9)$$

$$OH^\bullet + e^- \rightarrow OH^- \quad E^0 = 1.64 \text{ V } \textit{vs.} \text{ NHE} \quad (10)$$

$$H_2O_2 + e^- + 2H^+ \rightarrow 2H_2O \quad E^0 = 1.77 \text{ V } \textit{vs.} \text{ NHE} \quad (11)$$

$${}^\bullet OH + e^- + H^+ \rightarrow H_2O \quad E^0 = 2.33 \text{ V } \textit{vs.} \text{ NHE} \quad (12)$$

From a thermodynamic perspective, the production of hydrogen through the decomposition of ammonia (eqn (13) and (14)) is more favorable compared to water splitting (eqn (1) and (2)).[63,64]

$$\frac{2}{3}NH_3(g) \rightarrow H_2(g) + \frac{1}{3}N_2(g) \quad \Delta G^0 = +11 \text{ kJ mol}^{-1} \quad (13)$$

$$\frac{2}{3}NH_3(aq) \rightarrow H_2(g) + \frac{1}{3}N_2(g) \quad \Delta G^0 = +18 \text{ kJ mol}^{-1} \quad (14)$$

Notably, photocatalytic reactions involving ammonia are feasible only when the reduction and oxidation potentials of ammonia fall between the semiconductor's conduction band (CB) and valence band (VB) potentials. During this process, various nitrogen-containing products such as N_2, NO_2^-, NO_3^-, and NO_x can be formed owing to their closely related redox potentials. The specific potentials of these reactions are detailed in eqn (15)–(20)[65] and Fig. 2(a). Technically, ammonia decomposition can yield varying quantities of different products depending on several reaction parameters such as pH, temperature, initial ammonia or O_2 concentration, and the presence of trapping or sacrificial agents. For an effective photocatalytic cracking of ammonia, the photo-generated

Open Access Article. Published on 04 apríl 2025. Downloaded on 28.01.2026 06:48:11.
This article is licensed under a Creative Commons Attribution-NonCommercial 3.0 Unported Licence.

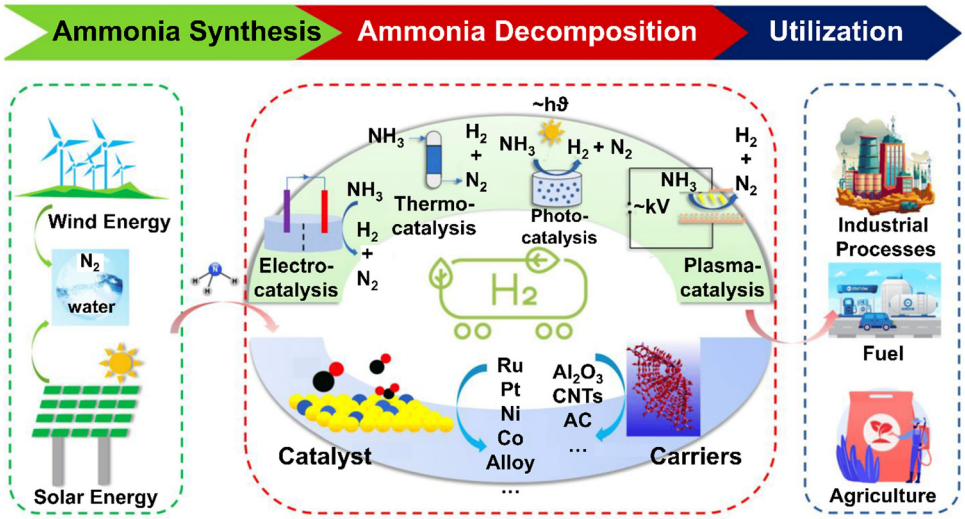

Fig. 1 The status of hydrogen generation from ammonia decomposition. This figure was adapted with permission from ref. 56. Copyright 2023, MDPI.

electrons and holes on the semiconductor surface must possess appropriate reduction and oxidation capabilities. These enable reactions with species adsorbed on the catalyst surface, such as O_2, NH_4^+, NO_2^-, and NO_3^-, facilitating the generation of free radicals or diverse products.

$$6H_2O_{(l)} + 6e^- \rightarrow 3H_{2(g)} + 6OH^-_{(aq)} \quad \text{Cathode} \quad (15)$$

$$2NH_4^+{}_{(aq)} + 8OH^-_{(aq)} \rightarrow N_{2(g)} + 8H_2O_{(l)} + 6e^- \quad \text{Anode} \quad (16)$$

$$2NH_4^+{}_{(aq)} + 2OH^-_{(aq)} \rightarrow N_{2(g)} + 3H_{2(g)} + 2H_2O_{(l)} \quad \text{Full cell,}$$
$$E_{cell} = 0.27 \text{ V } \textit{vs.} \text{ SHE} \quad (17)$$

$$8H_2O_{(l)} + 8e^- \rightarrow 4H_{2(g)} + 8OH^- \quad \text{Cathode} \quad (18)$$

$$NH_4^+{}_{(aq)} + 10OH^-_{(aq)} \rightarrow NO_3^-{}_{(aq)} + 7H_2O_{(l)} + 8e^- \quad \text{Anode} \quad (19)$$

$$NH_4^+{}_{(aq)} + 2OH^-_{(aq)} + H_2O_{(l)} \rightarrow NO_3^-{}_{(aq)} + 4H_{2(g)}$$
$$\text{Full cell, } E_{cell} = 0.88 \text{ V } \textit{vs.} \text{ SHE} \quad (20)$$

Furthermore, the photocatalytic decomposition of ammonia typically ceases under acidic conditions, suggesting that H^+ ions impede the transformation of ammonia into NH_2 free radicals. As the pH increases, ammonia is likely to react with surrounding oxygen, forming NO_2^-, NO_3^-, and other nitrogen oxides and adversely affecting hydrogen production. In addition, many photocatalysts currently face significant challenges with carrier recombination and poor light-harvesting efficiency. Consequently, the development of more effective photocatalytic materials remains crucial for the advancement of ammonia treatment through photocatalysis.[68]

To date, only a group of photocatalysts, such as TiO_2, ZnO, ZnS, Mo_2N, graphene, and their metal-loaded hybrid materials, have been found effective in decomposing aqueous ammonia solutions.[56] However, their hydrogen production rate, capped at 15.56 μmol g^{-1} min^{-1}, remains insufficient to satisfy practical application requirements.[67] To address this shortcoming, Utsunomiya *et al.*[19] investigated the photocatalytic performance of Ni/TiO_2 catalysts toward ammonia decomposition and explored the mechanism of NH_3 breakdown by proposing three distinct reaction pathways (Fig. 2(b)). These pathways involved the formation of N_2 and H_2 through intermediates radicals: route 1 entailed the formation of NH radicals *via* the removal of one hydrogen atom from two NH_2 radicals; route 2 involved the direct coupling of adjacent NH_2 radicals to form NH_2–NH_2; and route 2′, where NH_2–NH_2 formation occurred through the interaction of H_2N–NH_3. The activation energies for routes 1 and 2 were determined to be 236 kcal mol^{-1} and 74.8 kcal mol^{-1}, respectively, with route 2 being more energetically favorable. Additionally, the pathways for N_2 and H_2 formation *via* NH_2–NH_2 coupling were further delineated into route 2, which involved the coupling of NH_2 radicals to form H_2N–NH_2, and route 2′, where NH_2 interacted with an NH_3 molecule in the gas phase.

Alternatively, beyond photocatalysis, solar heating catalysis demonstrates the highest efficiency in sunlight utilization (approaching 100%) and can achieve temperatures up to 400 °C. This facilitates the heating of catalysts for thermocatalysis under natural solar irradiation. In the context of solar-powered ammonia decomposition, cobalt-based catalysts are preferred due to their abundance and effectiveness.[67] Yuan *et al.*[67] developed a catalyst by immobilizing single atoms of cobalt on cerium dioxide nanosheets (SA Co/CeO_2) (Fig. 2(c) and (d)) for photocatalytic degradation of ammonia in tubular reactor at low temperatures (Fig. 2(e)). As can be seen in Fig. 2(f), integrated with a custom-built TiC/Cu-based solar-heating device, the SA Co/CeO_2 demonstrated a stable hydrogen generation rate of 2.7 mmol g^{-1} min^{-1} under 2 suns irradiation, which is 572 times more effective than traditional weak sun-light-driven NH_3 decomposition. The hydrogen produced was found to be sufficiently pure to power a hydrogen fuel cell without further purification directly. Theoretical calculations revealed that SA Co/CeO_2 significantly lowers the energy barrier for nitrogen binding during ammonia decomposition, thereby enhancing the reaction's progress (Fig. 2(g)).

 This journal is © The Royal Society of Chemistry 2025

Open Access Article. Published on 04 apríl 2025. Downloaded on 28.01.2026 06:48:11.
This article is licensed under a Creative Commons Attribution-NonCommercial 3.0 Unported Licence.

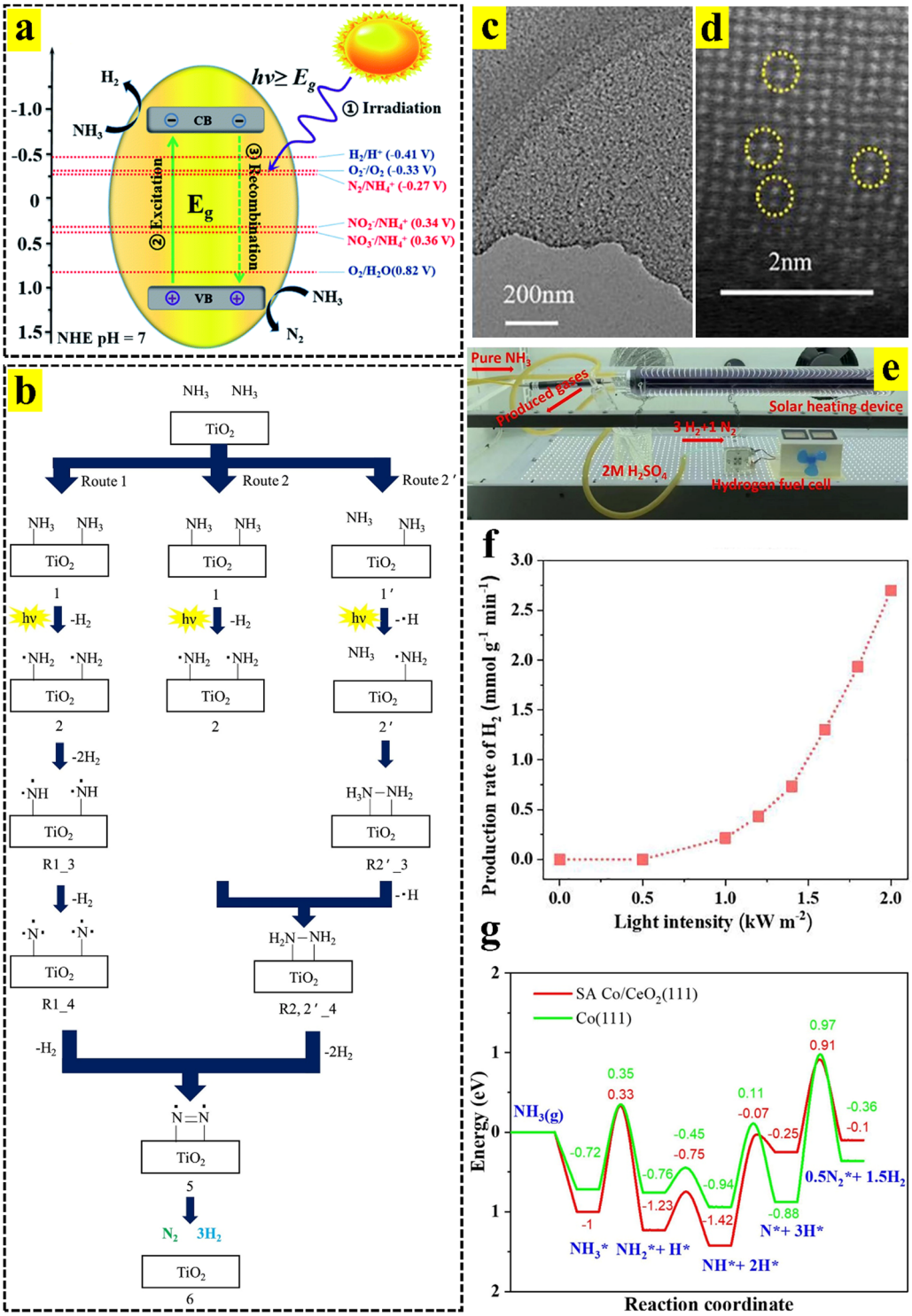

Fig. 2 (a) Schematic process of photocatalytic NH_3 decomposition. This figure was adapted with permission from ref. 66. Copyright 2020, Royal Society of Chemistry. (b) Proposed reaction mechanism for NH_3 decomposition to N_2 and H_2 on the TiO_2 photocatalyst. This figure was adapted with permission ref. 19, Elsevier. (c) TEM image and (d) HAADF-STEM image of SA Co/CeO_2. (e) Photograph of SA Co/CeO_2 loaded in a novel solar-heating device to drive hydrogen fuel cell under 2 solar irradiation. (f) H_2 production rate from NH_3 decomposition by SA Co/CeO_2. (g) Energy profiles of NH_3 decomposed as H_2 and N_2 on SA Co/CeO_2 (111) and Co (111) surfaces. These figures were adapted with permission from ref. 67. Copyright 2023, Elsevier.

Moreover, Lin *et al.*[69] employed a straightforward nebulization-coating technique to immobilize a wide array of single-atom transition metals (TMs: Co, Mn, Fe, Ni, and Cu) on microporous carbon nitride (MCN) (Fig. 3(a)), creating catalyst panels designed for solar-light-driven photocatalytic gaseous ammonia splitting (Fig. 3(b)). Under ambient conditions, the optimized Ni-MCN

Open Access Article. Published on 04 apríl 2025. Downloaded on 28.01.2026 06:48:11.
This article is licensed under a Creative Commons Attribution-NonCommercial 3.0 Unported Licence.

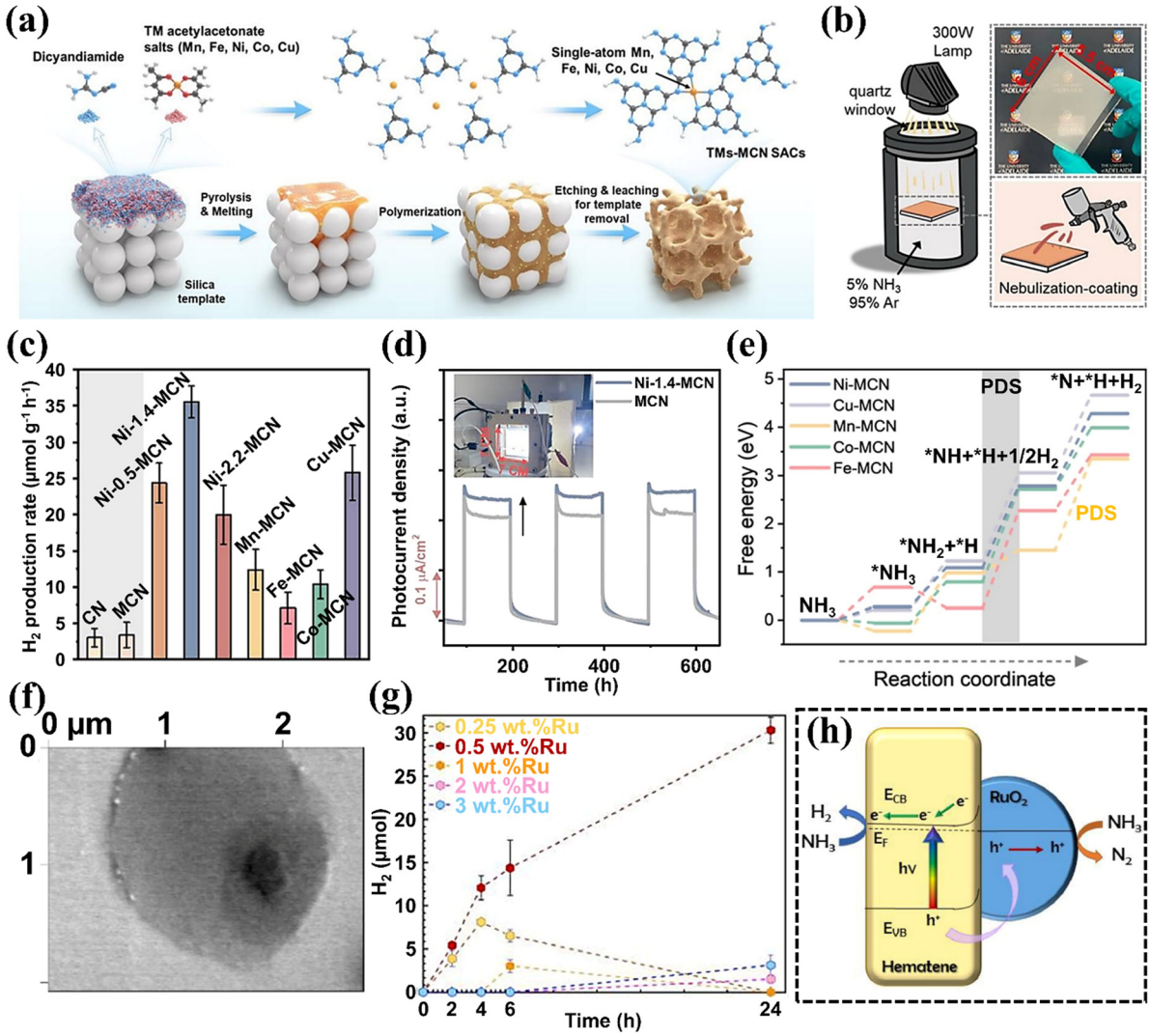

Fig. 3 (a) Schematic of the synthesis procedure of TMs-MCN SACs. (b) Illustration of the reaction system and the nebulization-coating method for fabricating TM-MCN panels. (c) Rates of H_2 production by CN, MCN, and Ni-MCNs with different Ni loadings and TMs MCNs (TMs = Mn, Fe, Co, Ni, Cu, with a similar loading percentage of ~1.4 wt%). (d) Photocurrent responses of MCN and Ni-1.4-MCN (inset: picture of the large-sized cell). (e) Energy profiles for the reaction process. These figures were adapted with permission from ref. 69. Copyright 2023, American Chemical Society. (f) Correlative probe and electron microscopy image of hematene sheet. (g) Decomposition of ammonia over Ru-hematene samples to optimize weight loading of Ru. (h) Schematic mechanism of ammonia decomposition by the Ru-hematene photocatalyst. These figures were adapted with permission from ref. 70. Copyright 2023, Elsevier.

demonstrated a hydrogen production rate of 35.6 μmol g^{-1} h^{-1}, significantly outperforming pure MCN (by approximately 14-fold) and other composite alternatives (Fig. 3(c)). This enhanced photocatalytic activity and photocurrent response (Fig. 3(d)) can be attributed to the presence of Ni–N_4 sites, which enhance the optical properties, expedite charge carrier separation/transfer, and improve the kinetics of ammonia splitting on the catalysts. Regarding Fig. 3(e), the Ni site on MCN is the most favorable for NH_3 splitting among all these TMs due to its lowest free energy increase in the potential-determining step (PDS).

In another study, Dzíbelová *et al.*[70] utilized an ultrasound-supported exfoliation technique to anchor ruthenium oxide nanoparticles onto 2D hematene (α-Fe_2O_3) (Fig. 3(f)) for the decomposition of an aqueous ammonia solution into hydrogen and nitrogen under visible light irradiation. Experimental results demonstrated that with an optimal ruthenium dosage of 0.5 wt%, the Ru-hematite, after 24 hours, achieved a hydrogen yield that was 2.5 times higher than that of pure hematene (Fig. 3(g)), attributed to the enhanced generation of electrons and holes (Fig. 3(h)). Moreover, without any cleaning interventions, the Ru-hematite photocatalyst exhibited only an 11% reduction in photocatalytic activity after five consecutive runs, suggesting its suitability for practical applications.

3. Electrocatalysis

Recently, hydrogen generation through electrochemical reactions, such as ammonia decomposition by electrocatalysis at

 This journal is © The Royal Society of Chemistry 2025

Open Access Article. Published on 04 aprel 2025. Downloaded on 28.01.2026 06:48:11.
This article is licensed under a Creative Commons Attribution-NonCommercial 3.0 Unported Licence.

moderate temperatures, has attracted more attention.[71] However, electrocatalytic ammonia decomposition faces challenges such as high overpotentials, unfavorable thermodynamics, and slow reaction kinetics.[72] Based on the different existing states of NH_3, electrochemical ammonia decomposition can be categorized into the electrolysis of (i) aqueous ammonia solution, or (ii) liquid ammonia. In the electrolysis of alkaline aqueous ammonia solutions, NH_3 undergoes oxidation in the existence of OH^- ions at the anode (eqn (21)),[73] whereas H_2O can be reduced at the cathode (eqn (22) and (23)).[71,74,75]

$$2NH_3 + 6OH^- \rightarrow N_2 + 6H_2O + 6e^- \quad \text{Anode, } E^0 = -0.77 \text{ V } \textit{vs.} \text{ SHE} \tag{21}$$

$$6H_2O + 6e^- + 3H_2 + 6OH^- \quad \text{Cathode, } E^0 = -0.83 \text{ V } \textit{vs.} \text{ SHE} \tag{22}$$

$$2NH_3 \rightarrow N_2 + 3H_2 \quad \text{Overall, } E_{cell} = 0.06 \text{ V} \tag{23}$$

In 2002, Zisekas *et al.*[76] utilized silver as the reactor electrode to conduct the first tests on hydrogen production *via* electrocatalytic decomposition of ammonia. These tests demonstrated that NH_3 conversion efficiency ranged between 25 and 35% at temperatures of 773–873 K, indicating that reactor temperatures remained relatively high. It is well accepted that the energy density of hydrogen in liquid ammonia [NH_3(l), 3.6 kW h L^{-1}] is significantly higher compared to that in alkaline aqueous ammonia solution [NH_3(aq), 1.0 M, 0.1 kW h L^{-1}]. Fundamentally, the electrolysis of liquid ammonia differs from that of aqueous ammonia solutions, as both the anodic and cathodic half-reactions in liquid ammonia avoid the excessive oxidation of NH_3 that typically occurs in the presence of water.[71] Furthermore, the gravimetric H_2 density is as low as 6.1 mass% according to its solubility in water, 34.2 mass% at 20 °C.[77] Accordingly, Hanada *et al.*[78] evaluated the direct electrolysis of liquid ammonia, where alkaline metal amides (MNH_2, M = Li, Na, K) were utilized as the supporting electrolyte. Amides such as $LiNH_2$, $NaNH_2$, KNH_2, and *N*,*N*-dimethylformamide have enabled the electrolysis of liquid ammonia.[79] This process was conducted at exceptionally low temperatures, ranging from −70 to −65 °C, using pure platinum electrodes.[80]

Moreover, during electrocatalytic reaction, NH_3 can be converted aqueous to NO_3^- and then to products such as HNO_2, NO, NH_2OH, NH_3, N_2O, and N_2 (eqn (24)–(30)). Generated nitrogen is benign and easily separable, and is the most stable nitrate reduction product with a standard redox potential (E^0) of 1.25 V *vs.* RHE.[72]

$$NH_{3(aq)} + 3H_2O(l) \rightarrow NO^-_{3(aq)} + 9H^+ + 8e^- \quad E^0 = 0.82 \text{ V } \textit{vs.} \text{ RHE} \tag{24}$$

$$NO^-_{3(aq)} + 2H^+ + 2e^- \rightarrow NO^-_{2(aq)} + H_2O_{(l)} \quad E^0 = 0.85 \text{ V } \textit{vs.} \text{ RHE} \tag{25}$$

$$NO^-_{3(aq)} + 3H^+ + 2e^- \rightarrow HNO_{2(aq)} + H_2O_{(l)} \quad E^0 = 0.89 \text{ V } \textit{vs.} \text{ RHE} \tag{26}$$

$$NO^-_{3(aq)} + 4H^+ + 3e^- \rightarrow NO_{(aq)} + 2H_2O_{(l)} \quad E^0 = 0.96 \text{ V } \textit{vs.} \text{ RHE} \tag{27}$$

$$NO^-_{3(aq)} + 7H^+ + 6e^- \rightarrow NO_2OH_{(aq)} + 2H_2O_{(l)} \quad E^0 = 0.67 \text{ V } \textit{vs.} \text{ RHE} \tag{28}$$

$$2NO^-_{3(aq)} + 10H^+ + 8e^- \rightarrow N_2O_{(g)} + 5H_2O_{(l)} \quad E^0 = 1.12 \text{ V } \textit{vs.} \text{ RHE} \tag{29}$$

$$2NO_3^-{}_{(aq)} + 12H^+ + 10e^- \rightarrow N_{2(g)} + 6H_2O_{(l)} \quad E^0 = 1.25 \text{ V } \textit{vs.} \text{ RHE} \tag{30}$$

Technically, the electrocatalytic decomposition of NH_3 encompasses two primary phases: (i) the ammonia oxidation reaction (AOR) and (ii) the hydrogen evolution reaction (HER). An effective high-efficiency electrocatalyst should be capable of catalyzing both the AOR and HER at a low potential.[36] Despite its potential, the activity level of AOR is insufficient for low-temperature operations. The AOR integrates more easily with fuel cell technologies and provides a more effective method for hydrogen generation than water electrolysis, which represents the second most common hydrogen production method and accounts for approximately 4% of global hydrogen production. In addition, water electrolysis, which is not thermodynamically favored, theoretically necessitates applying a voltage as high as 1.23 V to break down highly stable water molecules, requiring about 180 MJ of energy to produce 1 kg of H_2. In contrast, the AOR has a significantly lower energy requirement of approximately 33 MJ per kg of hydrogen generated.[81]

Research has demonstrated that the electrocatalytic activity for ammonia oxidation correlates with the surface properties of materials. The catalyst remains active when intermediate NH_x species are present but becomes inhibited when strongly binding nitrogen species are formed.[82] In this context, the widely accepted mechanism was proposed by Gerischer and Mauerer in 1970, with the fundamental steps detailed in eqn (31)–(35). Briefly, NH_3 can be deprotonated in the presence of hydroxyl ions in eqn (31)–(33), producing water molecules while simultaneously releasing an electron at each step. N* adatoms (formed in eqn (33)) are surface poisons because of a typically large kinetic barrier for N–N bond formation and release nitrogen. Thus, adsorbed NH_x (and NH_y) species can interact with one another to form an N–N bond, subsequently generating an H_xNNH_y species (eqn (34)). Regarding the Gerischer–Mauerer mechanism, these species are then deprotonated to N_2, which desorbs from the surface; however, the identity of the NH_x and NH_y species that react to form the N–N bond remains in dispute (eqn (35)).[83]

$$NH_3 + OH^- + * \rightarrow NH_2* + H_2O + e^- \tag{31}$$

$$NH_2* + OH^- + * \rightarrow NH* + H_2O + e^- \tag{32}$$

$$NH* + OH^- + * \rightarrow N* + H_2O + e^- \tag{33}$$

$$NH_x* + NH_y* \rightarrow H_xNNH_y* + * \tag{34}$$

$$H_xNNH_y* + (x+y)OH^- \rightarrow N_2 + (x+y)H_2O + (x+y)e^- + * \tag{35}$$

The catalytic activity can be substantially enhanced when a portion of the metal is utilized as an electrode by applying a current or potential between the catalyst and a counter electrode deposited on the solid electrolyte.[36] To date, a diverse

Open Access Article. Published on 04 apríl 2025. Downloaded on 28.01.2026 06:48:11.
This article is licensed under a Creative Commons Attribution-NonCommercial 3.0 Unported Licence.

range of materials, such as noble metals, metal oxides, and non-metals, have demonstrated high catalytic activity for ammonia electro-oxidation. Notably, Pt has emerged as the most effective electrocatalyst for this reaction. However, most ammonia electro-oxidation systems necessitate strong alkaline media (such as NaOH), leading to rapid deactivation and poisoning of Pt catalysts, as well as oxygen evolution and NO_x production. Under strongly alkaline conditions, electrodeposited Pt-based electrodes and nanotubes have effectively oxidized ammonia into hydrogen.[80]

In this context, Herron *et al.*[83] examined AOR efficiency on various face-centered cubic (fcc) metals (Au, Ag, Cu, Pd, Pt, Ni, Ir, Co, Rh, Ru, Os, and Re) using density functional theory (DFT) calculations. They reported that Pt exhibited the most promising catalytic activity, followed by Ir and Cu, due to its low onset potential (Fig. 4(a) and (b)). It was found that adsorbed NH_2 was the dominant intermediate, facilitating the preferred N–N bond formation both kinetically and thermodynamically (Fig. 4(c)). In another study, Zhong *et al.*[82] investigated catalytic electro-oxidation of liquid ammonia using transition metal dimers (Fe_2, Co_2, Ru_2, Rh_2, and Ir_2) anchored on graphite-carbon nitride monolayers (TM_2@g-CN). Their findings reinforce the mechanism proposed by Gerischer and Mauerer, where N–N bond formation is facilitated by hydrogenated NH_x species rather than N adatoms (Fig. 4(d)). Importantly, catalytic activity studies demonstrated that Fe, Co, Ru, Rh, and Ir anchored in g-CN monolayers are exceptionally promising AOR catalysts due to their low limiting potentials of −0.47, −0.5, −0.48, −0.52, and −0.48 V, respectively. Among them, Ir_2@g-CN, as a bifunctional catalyst for electrocatalytic NH_3

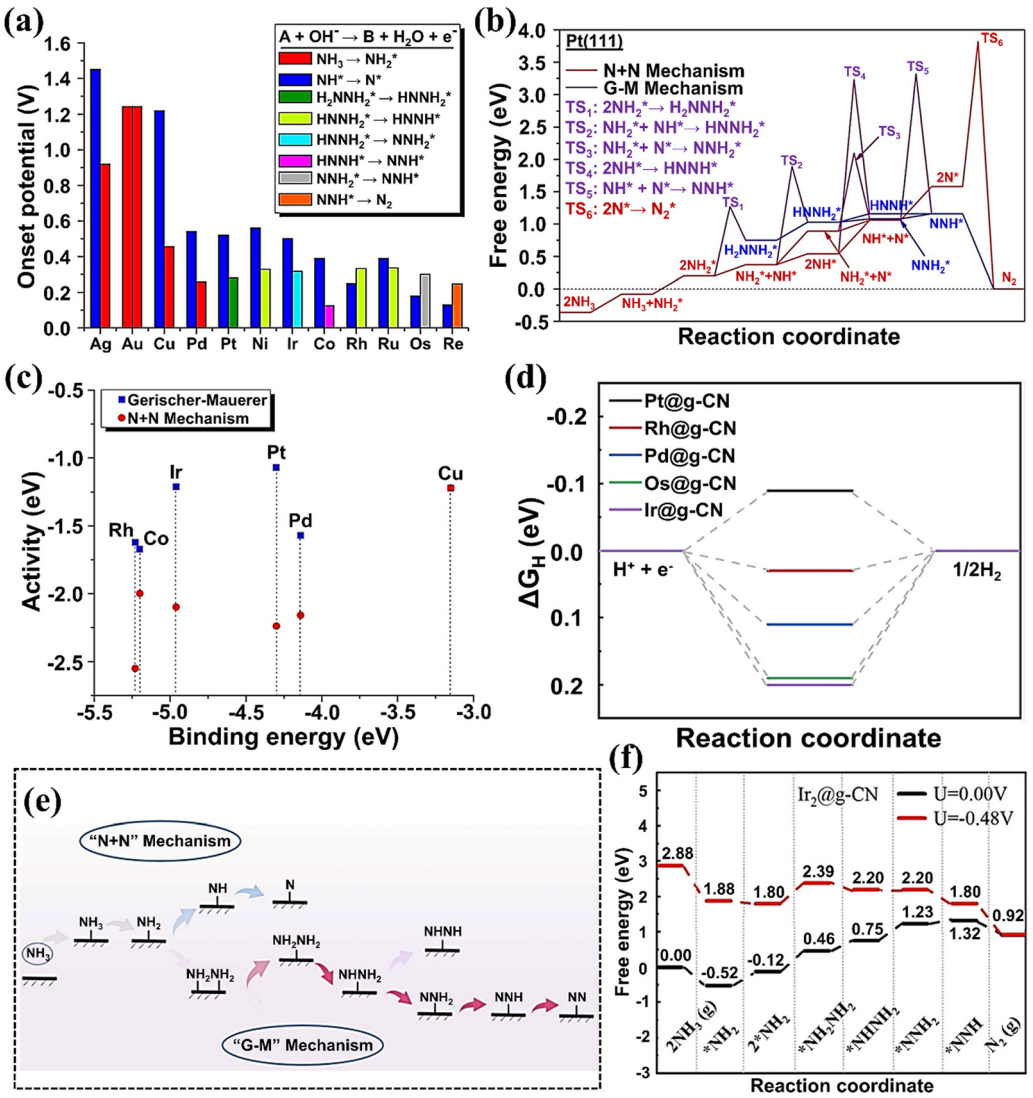

Fig. 4 (a) Estimated onset potential for close-packed facets of transition metals. (b) Activity as predicted by Sabatier analysis for both mechanisms at 0 V_{RHE}. (c) Free-energy diagram for ammonia electro-oxidation on Pt(111) at 0 V_{RHE}. These figures were adapted with permission from ref. 83. Copyright 2015, American Chemical Society. (d) Proposed mechanism for the AOR on TM_2@g-CN. (e) The calculation free energy diagram of the AOR through the Gerischer–Mauerer mechanism over Ir_2@g-CN at different applied potentials. (f) The calculated free energy diagram of the HER on TM_2@g-CN samples. These figures were adapted with permission from ref. 82. Copyright 2023, Elsevier.

 This journal is © The Royal Society of Chemistry 2025

Open Access Article. Published on 04 apríl 2025. Downloaded on 28.01.2026 06:48:11.
This article is licensed under a Creative Commons Attribution-NonCommercial 3.0 Unported Licence.

decomposition, showed low energy barriers of 0.48 eV and 0.20 eV for the AOR (Fig. 4(e)) and HER (Fig. 4(f)), respectively. It was observed that modulating TM atoms with varying d-electron numbers allows for tuning the d-band center (ε_d) of TM atoms on TM_2@g-CN composites, providing a predictive measure for AOR performance and offering theoretical guidance for designing advanced AOR electrocatalysts.

In Modisha's study,[84] decomposition of ammonia using a Pt–Ir electrocatalyst was investigated in a potassium hydroxide (KOH, 5 M) solution (Fig. 5(a)). This research demonstrated that the current density of NH_3 electro-oxidation reaction rose at high temperature and ammonia concentration, achieving a peak ammonia conversion of 78% at 2300 ppm (Fig. 5(b)). From Fig. 5(c), the highest hydrogen flow rate recorded was 25 L h^{-1}, with an associated energy consumption of 1.6 W h L^{-1} H_2^{-1}. The purity of hydrogen, as determined by gas chromatography, was found to be 86%. Moreover, Dong *et al.*[85] synthesized five types of electrocatalysts, including Pt-black, Rh, Pt–Ir, Rh–Pt, and Rh–Pt–Ir alloys, aimed at reducing the overpotential of the anode reaction for ammonia cracking (Fig. 5(d)). These alloys were electrochemically evaluated for their efficacy in ammonia decomposition in the presence of NH_4Cl. The trimetallic Rh–Pt–Ir and the bimetallic Pt–Ir, as well as the Rh-contained alloy electrodes, demonstrated enhanced activity and reduced deactivation. Notably, the Rh–Pt–Ir alloy anode (Fig. 5(e)) exhibited the highest electrocatalytic performance, achieving the lowest minimum potential (E_{min}) of

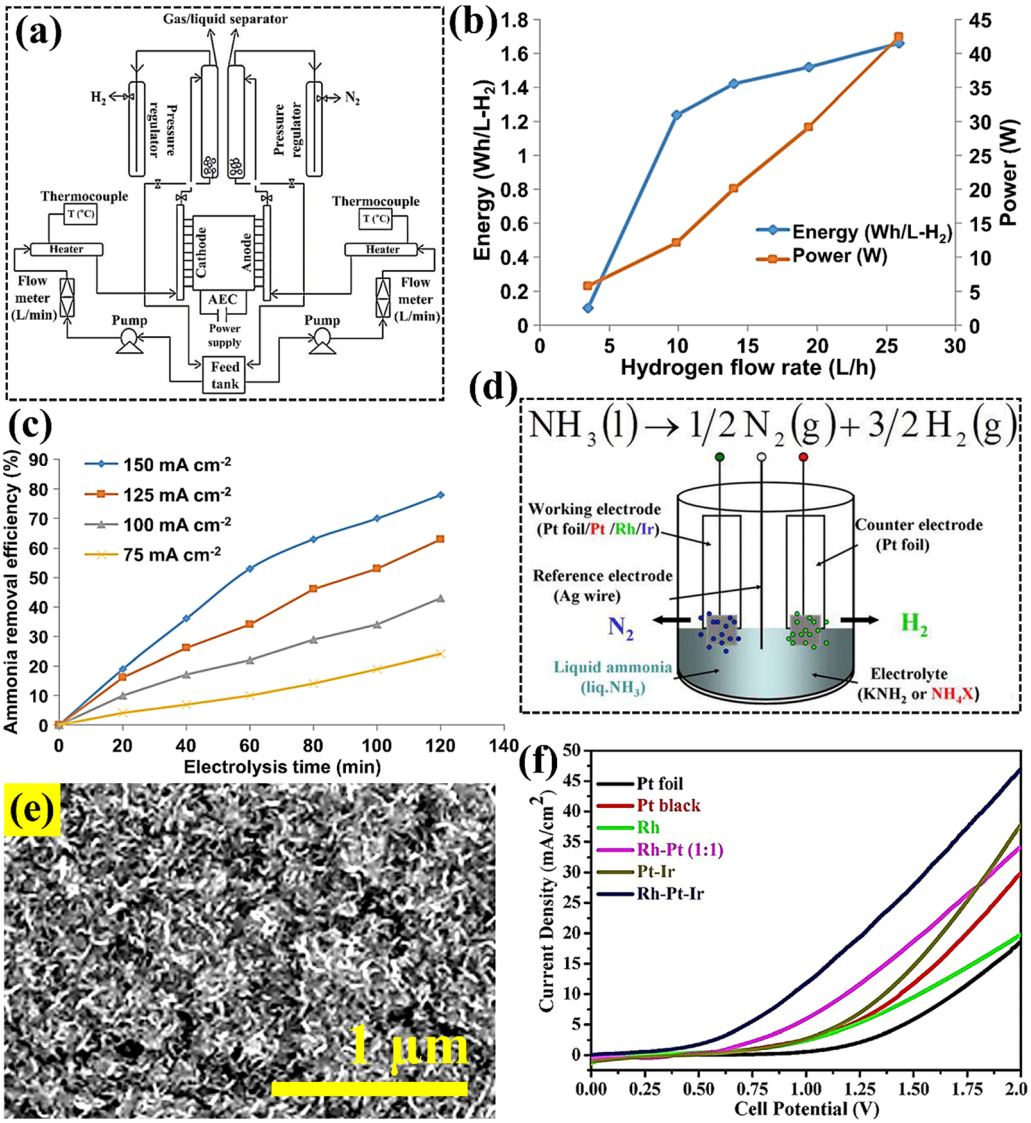

Fig. 5 (a) Schematic representation of the ammonia electrolysis process for hydrogen production. (b) Volumetric hydrogen generation rates and the required energy and power input (cell retention time (R_t): was 12.5 min, 2000 ppm NH_3 in 5 M KOH at 55 °C). (c) Ammonia decomposition efficiency as a function of time and current density. These figures were adapted with permission from ref. 84. Copyright 2016, Elsevier. (d) Schematic electrolysis of liquid ammonia using different ammonium salt electrolytes with the reference electrode. (e) SEM image of the freshly prepared Rh–Pt–Ir electrocatalyst. (f) Cyclic voltammetry curves of NH_3 (l) with 1 M NH_4Cl in a two-electrode system. These figures were adapted with permission from ref. 85. Copyright 2016, Elsevier.

Open Access Article. Published on 04 aprel 2025. Downloaded on 28.01.2026 06:48:11.
This article is licensed under a Creative Commons Attribution-NonCommercial 3.0 Unported Licence.

approximately 0.47 V and the highest current density of 46.9 mA cm^{-2} at 2.0 V (Fig. 5(f)). The results of this research reflect that the energy required for hydrogen generation from the electrocatalysis of liquid NH_3 can be significantly lowered through strategic selection and compositional optimization of alloy catalysts.

4. Plasma

As mentioned earlier, significant research efforts have been directed toward developing alternative energy supply methods for ammonia decomposition. These methods include the use of electric currents,[86] electron beams,[87] microwaves,[88] and plasma,[89] which offer higher conversion rates at lower temperatures compared to traditional thermocatalysis. Among them, there has been a notable shift towards exploring non-thermal plasma (NTP) for catalytic ammonia decomposition at low temperatures. This approach potentially enhances the response time and modularity of ammonia-based hydrogen production systems, thereby improving their applicability in sectors like transportation.[90]

Plasma is generally defined as a state of gas where the atoms are partially or fully ionized, maintaining overall electrical neutrality, containing a large number of highly energetic

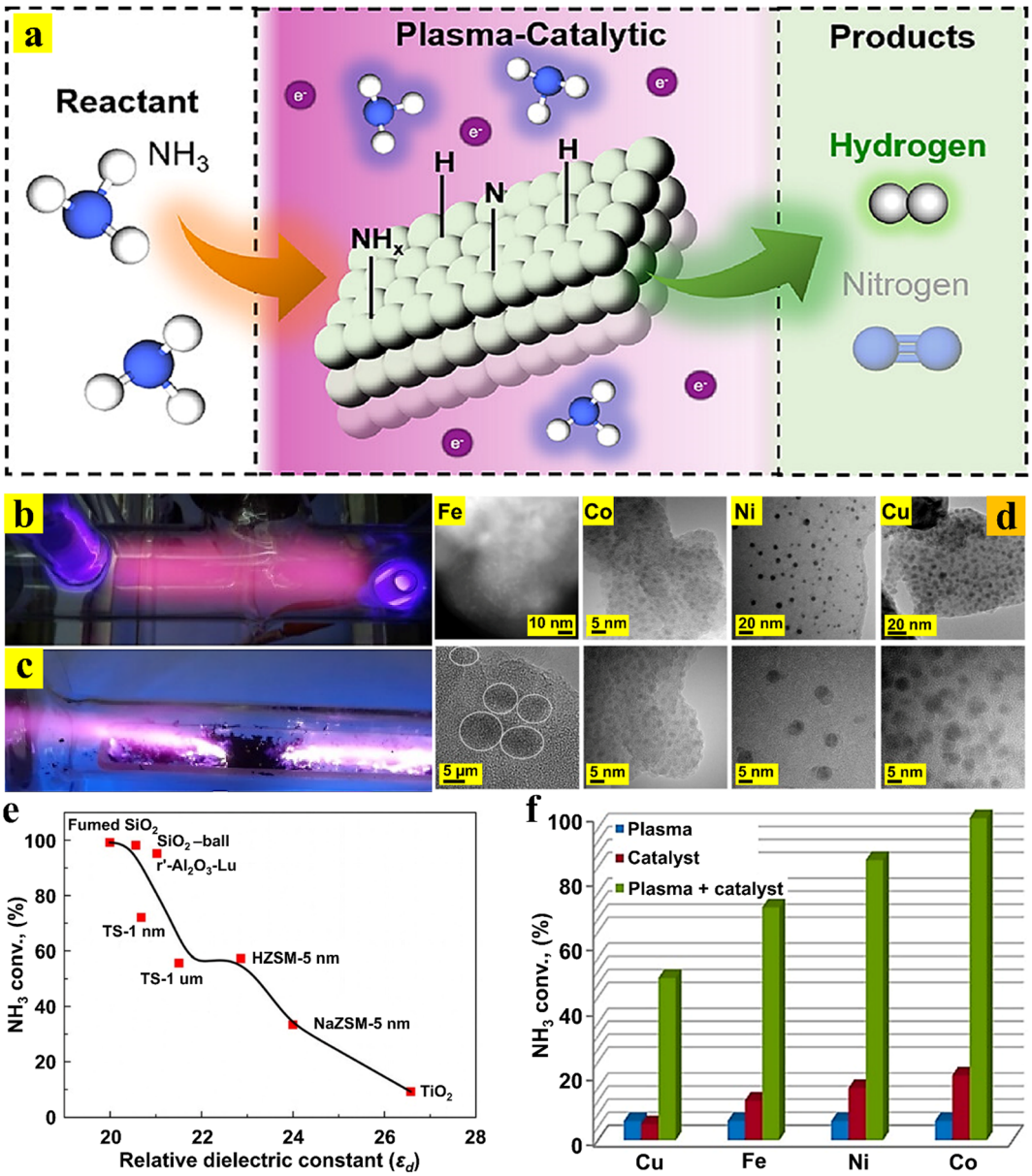

Fig. 6 (a) Schematic representation of the plasma-catalytic NH_3 decomposition. This figure was adapted with permission from ref. 94. Copyright 2024, American Chemical Society. *In situ* plasma-assisted catalytic NH_3 conversion system (b) under NTP conditions and (c) glow discharge reactor. These figures were adapted with permission from ref. 95. Copyright 2022, MDPI. (d) TEM micrographs of Fe, Co, Ni, and Cu catalysts supported on fumed SiO_2 (reduced in H_2 plasma). (e) NH_3 conversions on Co catalysts on various supports as a function of relative dielectric constants of supports in plasma + catalyst mode (NH_3 feed 40 mL min^{-1}, temperature 450 °C, supported catalyst 0.88 g, discharge gap 3 mm, discharge frequency 12 kHz). (f) Influence of metals on NH_3 conversion in plasma + catalyst, plasma, and catalyst modes (similar condition for 3b). These figures were adapted with permission from ref. 94. Copyright 2024, American Chemical Society.

 This journal is © The Royal Society of Chemistry 2025

Open Access Article. Published on 04 aprel 2025. Downloaded on 28.01.2026 06:48:11.
This article is licensed under a Creative Commons Attribution-NonCommercial 3.0 Unported Licence.

electrons and reactive species (*e.g.*, excited molecules, atoms, ions, and radicles) (Fig. 6(a)–(c)).[9,91,92] It was found that integrating non-thermal plasma with a catalyst can significantly modify the catalytic reaction pathway, leading to enhanced selectivity or reaction rates through the interaction of plasma, reactant, and catalyst.[91] Notably, the H_2 energy yield from the plasma catalysis method is nearly five times greater than that achieved through thermocatalysis. This indicates that plasma catalysis substantially enhances the economic efficiency of hydrogen production from ammonia.[9] In 2006, research on the impact of dielectric barrier discharge plasma on ammonia decomposition revealed that using a commercially available bulk Fe-based catalyst significantly increased NH_3 conversion rates. Specifically, NH_3 conversion escalated from 7.4% to 99.9% when the Fe-based catalyst was positioned within a plasma zone at 410 °C.[93] In this context, the researchers further optimized the ammonia decomposition process by utilizing low-temperature plasma, either using high-performance catalysts or by identifying optimal reaction conditions.

In 2015, Wang *et al.*[93] conducted a comparative study on the efficiencies of hydrogen generation from ammonia using both thermal and plasma catalysis methods over different low-cost metal catalysts (Fe, Co, Ni, Cu) on a fumed SiO_2 support (Fig. 6(d)). The results indicated that the NH_3 conversion strongly depends on the metal–N bond strengths and on the relative dielectric constant (ε_d) of the support in the plasma reaction. It was observed that the moderately strong Co–N bonds can be expected to improve the plasma–catalyst synergy, thus leading to higher NH_3 conversions (Fig. 6(e)). Notably, the relative ε_d of the support can efficiently contribute to plasma-catalytic NH_3 decomposition performance. As shown in Fig. 6(f), a support with a small ε_d facilitates plasma-catalytic NH_3 decomposition. Technically, plasma gas discharge can rapidly heat the reaction/catalyst, enhancing the energy efficiency of hydrogen production. Additionally, plasma has been shown to facilitate the rate-limiting step by accelerating the recombinative desorption of N_{ad} from the catalyst bulk structure.[91] In another study, the effects of varying discharge zone lengths on the efficiency of plasma-catalytic ammonia decomposition at a set discharge frequency were investigated. The research revealed that doubling the discharge zone length from 3.0 cm to 3.5 cm at a frequency of 10 kHz resulted in a twofold increase in NH_3 conversion efficiency.[9] Consequently, these findings indicate that non-thermal plasma and catalysts can synergistically interact to efficiently convert NH_3 to H_2 under mild conditions. However, despite the potential of plasma-catalytic processes, the number of catalysts tested and evaluated remains limited compared to those used in thermocatalysis.

Tables 2–4 summarize the literature on hydrogen generation from ammonia cracking through photocatalytic, electrocatalytic, and plasma processes, respectively.

5. Other approaches

It is well accepted that the alternative methods for ammonia decomposition, such as electrocatalysis and photocatalysis, often depend on complex catalysts that include costly precious metals. While non-precious metals are more affordable, they tend to exhibit lower catalytic efficiencies and reduced stabilities.[112] To tackle the challenges in conversion performance, recently, ammonia–water has been recognized as a promising liquid hydrogen carrier with the potential for widespread use in hydrogen generation. However, the hydrogen derived from ammonia–water still poses major challenges. Despite advancements in various methods to enhance the efficiency of H_2 production from ammonia–water, these techniques have yet to reach a level that is suitable for practical industrial applications.[112] In this context, Yan *et al.*[112]

Table 2 Performance comparison of different catalysts toward photocatalytic NH_3 decomposition

Photocatalyst	Light source	Time	Initial NH_3 concentration	Maximum decomposition ability	Ref.
Pt–TiO_2 (0.5 wt% Pt)	450 W high pressure Hg lamp	24 h	5 mM	Over 95%	96
Ni/TiO_2 (0.5 wt% Ni)	500 W Xe lamp	3 h	5 mL, 0.59 mol L^{-1}	131.7 μmol H_2 per g-catalyst	19
Ce-doped TiO_2 (1.4 wt% Ce)	8 W Hg pen-ray lamp	10 h	100 mL, 0.8274 g L^{-1}	1010 mmol H_2 per g-catalyst	97
N–C@TiO_2	25 W UV lamp	5 min	100 μL aqueous ammonia (30%)	100%	98
MoS_2@TiO_2	25 W UV lamp	7 min	100 μL aqueous ammonia (30%)	91%	99
MoS_2/N-doped graphene	300 W UV-visible lamp	8 h	100.0 mg L^{-1}	99.6%	100
Nitrogen-doped rGO/TiO_2	8 W Hg pen-ray lamp	12 h	0.883 g L^{-1}	208 μmol h^{-1} g^{-1}	80
GQDs (graphene quantum dots)/CN (g-C_3N_4)	150 W Xe arc lamp	7 h	1.5 mg L^{-1}	90%	101
ZnO/Ag	300 W Xe lamp	2.5 h	1.5 mg L^{-1}	Circa 90%	102

Table 3 Performance comparison of different catalysts toward electrocatalytic NH_3 decomposition

Catalyst	Catalyst loading (mg cm^{-2})	Electrolyte	Onset potential	Current density (mA cm^{-2})	Scan rate (mV s^{-2})	Ref.
PtIr/C	2.00	1.0 M NH_3	0.470 V_{RHE}	—	10	103
RGO/Pt–Ir	—	1.0 M NH_4OH	−0.400 $V_{Ag/AgCl}$	20.00 at 0 $V_{Ag/AgCl}$	10	104
$Pt_{90}Ru_{10}$/C	1.00	1.0 M NH_4OH + 1.0 M KOH	—	0.920 at −0.210 $V_{Hg/HgO}$	20	105
Pt_xIr1_{00-x}/MgO	—	0.1 M NH_3 + 0.2 M NaOH	0.530 V_{RHE}	1.00 at 0.710 V_{RHE}	20	106
SnO_2–Pt/C	0.028	0.1 M NH_3 + 0.1 M KOH	0.450 V_{RHE}	1.62 at 0.690 V_{RHE}	20	53

Open Access Article. Published on 04 aprel 2025. Downloaded on 28.01.2026 06:48:11.
This article is licensed under a Creative Commons Attribution-NonCommercial 3.0 Unported Licence.

Table 4 Performance comparison of different catalysts toward plasma-assisted catalytic NH_3 decomposition

Catalyst	Power	Reactor configuration	Temperature (°C)	Pressure (bar)	Catalyst amount (g)	NH_3 flow rate (L min^{-1})	NH_3 conversion rate (%)	Ref.
FeO	12 kHz 26 W	DBD[a] reactor	410	—	10	0.04	>99.9	107
Ni–Al_2O_3	23.8 kHz 0–700 W	Non-thermal arc reactor	400–843	—	200	30.00	—	108
Ru–Al_2O_3	10 kHz 12–20 kV	DBD reactor	—	1	—	0.10–1.00	85.7	109
Metal–$MgAl_2O_4$	1.0–3.5 kHz 10–25 W	DBD reactor	—	1	—	1.00	82.0	110
No catalyst	10 kHz 3.5–22 kV	DBD reactor	—	—	—	0.50	13.0	111

[a] Note: dielectric barrier discharge.

developed a novel, eco-friendly, and ultrafast method for extracting hydrogen from ammonia–water without a catalyst and under ambient conditions using the laser bubbling in liquids (LBL) approach. This technique is entirely different from conventional catalytic methods for hydrogen extraction from ammonia–water. The LBL involves a focused pulsed laser directly beneath the surface of the liquid. When the pulsed laser is applied to ammonia–water, the molecules can be rapidly excited and ionized. This process generates cavitation bubbles at the focus point that achieve transient high temperatures, creating an optimal microspace for efficient hydrogen extraction. It was reported that the real adequate time of laser action on ammonia–water was just 0.36 ms per hour and the actual hydrogen yield reached 93.6 mol h^{-1} at laser "light-on" time, reflecting the acceptable efficiency of the LBL process.

Another attempt to develop a new approach toward ammonia decomposition was performed by McLennan and Greenwood,[113] discovering that electric discharge in a cathode ray tube can rapidly decompose ammonia. By eliminating the electric current, they focused on the decomposition using only high-speed electron beams, achieving up to 30% decomposition efficiency with pure ammonia. They also examined the effects of the presence of high-speed electrons (electron spark) on the reaction rate, noting ammonia dilution with N_2 enhanced the reaction while H_2 inhibited it. Similarly, Hirabayashi and Ichihashi[114] explored ammonia decomposition using ion beams on various catalysts, identifying vanadium and niobium nitrides ($V_nN_m^+$ and $Nb_nN_m^+$ (n = 3–6; $m = n$, $n - 1$)) as promising for hydrogen production.

6. Predicting NH_3 decomposition efficiency by machine learning

It is well recognized that the broad temperature range of the ammonia decomposition process in practical applications makes it difficult to monitor catalyst changes during the reaction, which is also a major barrier to its practical implementation.[115] In addition, discovery of catalysts for NH_3 decomposition is a crucial aspect and has traditionally relied on trial-and-error experiments.[115–117] Therefore, utilizing DFT and numerical modeling techniques can significantly accelerate research by validating the fundamental mechanisms of ammonia decomposition.[34]

In recent decades, machine learning (ML) technology has emerged as a powerful tool in designing novel catalysts, understanding composition-structure–property relationships, and analyzing complex data patterns. This efficient computational approach streamlines thermocatalytic ammonia decomposition while minimizing the need for extensive human and material resources in catalyst design.[115] The strength of ML algorithms lies in their capacity to learn from historical data without the need for explicit programming. This approach is anticipated to demonstrate high fidelity in identifying optimal operating conditions, not only for NH_3 cracking in the gas phase but also for optimizing CO_2 capture, hydrocracking, and dimethyl ether synthesis.[118]

To date, several studies have utilized ML models to identify and optimize catalysts for ammonia decomposition. For instance, Williams *et al.*[119] assessed the integration of ML with high-throughput experimentation to optimize catalyst compositions with low ruthenium content for NH_3 decomposition in a 16-channel parallel reactor system. They developed a model training in three progressive stages, utilizing datasets of 3, 22, and 28 catalysts. By analyzing the chemical properties of the secondary metal and reaction temperature, the model effectively predicted ammonia decomposition efficiency. It was found that by employing the random forest algorithm the catalyst performance was predicted with a mean absolute error of less than 0.16, demonstrating the approach's accuracy and reliability. In another study, Guo *et al.*[115] utilized ML using random forest regression, support vector machines, and gradient boost regression approaches to statistically analyze ammonia decomposition as a function of catalyst properties and reaction conditions. Their findings revealed a strong positive correlation between the catalytic efficiency and reaction temperature, with the gas hourly space velocity (GHSV) emerging as a key factor influencing both NH_3 conversion and H_2 production rates. Notably, optimal decomposition and hydrogen formation were achieved with a total metal loading below 20%wt. It was concluded that among the models tested, the gradient boost regression tree demonstrated strong predictive accuracy, achieving a coefficient of determination (R^2) greater than 0.85, a root mean square error (RMSE) below 13.24, and a mean absolute error (MAE) under 10.31.

Although ML has shown promising results, developed models often tend to be case-specific, limiting their

 This journal is © The Royal Society of Chemistry 2025

Open Access Article. Published on 04 aprel 2025. Downloaded on 28.01.2026 06:48:11.
This article is licensed under a Creative Commons Attribution-NonCommercial 3.0 Unported Licence.

generalizability across different catalyst systems. In addition, traditional ML-guided catalyst screening can be challenging to obtain new catalytic systems, specifically molecular catalysts for AOR electrocatalysts.[120] To address these theoretical limitations, recent studies have aimed to develop an ML model specifically designed to accurately predict the conversion of NH_3 to H_2. By compiling data from published literature, an extensive experimental database was established, and the relationship between independent variables and dependent responses was thoroughly evaluated using statistical analyses and mechanistic insights.[115]

Moreover, integrating reaction kinetics into the ML framework presents a promising research direction. In this context, understanding the role of reaction kinetics in predicting H_2 formation rates during NH_3 decomposition can provide valuable insights into catalyst behavior and improve predictive accuracy. Additionally, incorporating hydrogen inhibition effects into the ML model will enable researchers to better capture catalyst dynamics, ultimately enhancing performance predictions.[115] Notably, the exploration of advanced ML techniques can offer new insights into developing the connections among the characteristics of substances and their catalytic activity, selectivity, and stability of the complex catalytic systems.[121] In the future, with further research and widespread application of artificial intelligence technologies, ammonia decomposition processes are expected to become more efficient and environmentally sustainable, offering robust support for sustainable energy development.

7. Further challenges for ammonia decomposition

Extensive research has focused on developing highly active and durable catalysts for ammonia decomposition at minimal temperatures, intending to further lower the temperature to improve efficiency and promote environmentally sustainable processes. It is widely recognized that support materials for NH_3 decomposition catalysts should exhibit high basicity alongside high conductivity, low concentrations of electron-withdrawing groups, and extensive surface area. Increased basicity can enhance the dispersion of the active metal, thereby facilitating the dehydrogenation of ammonia and the recombinative desorption of surface nitrogen atoms, which are likely the rate-limiting steps of the reaction. Additionally, the electron-donating characteristics of the catalyst can indirectly interact with the support to promote stronger basicity. Consequently, adjusting the basicity of the supports is essential for developing efficient catalysts toward NH_3 decomposition. Beyond Ru and Ni catalysts, nitrides, carbides, and perovskites have also gained popularity for optimizing active components in catalytic processes. Looking ahead, it will be valuable to explore methods for separating and purifying hydrogen derived from ammonia decomposition in a cost-effective and highly efficient manner. Additionally, microwave and plasma-based decomposition of ammonia merits further investigation.

Moreover, the economic evaluation of a large-scale NH_3 decomposition plant has revealed a significant reliance on the cost of the green ammonia industry. It was demonstrated that lower costs of renewable energy and green ammonia production lead to reduced hydrogen production costs *via* NH_3 decomposition. With a baseline price of green ammonia set at 450 € per ton, the estimated levelized cost of hydrogen (LCOH) was approximately 4.82 € kg^{-1} (in 2019). However, this estimate is influenced by several uncertainties, including the accuracy of total investment cost estimation (±30%), the ammonia decomposition kinetics that affects cracker size and consumption, and the use of ammonia/hydrogen blends as fuel for endothermic reactions in conventional burners. In summary, if green ammonia becomes cost-competitive with fossil-based ammonia, with an estimated price range of 210–215 € ton^{-1}, the cost of producing pressurized hydrogen through ammonia decomposition would be approximately 3.00 € per kg, excluding any potential regulatory or financial incentives.[122]

8. Conclusions and perspectives

Ammonia, as an ideal hydrogen storage material, is expected to be used to address the challenges of hydrogen storage and transportation in the development of the hydrogen energy industry and overcome the safety problems related to hydrogen utilization. Although many ammonia-related studies have contributed to the promotion of ammonia as a favorable alternative renewable resource, further improvements are required in ammonia decomposition to make it a practical H_2 carrier option for on-site generation.

Currently, the great potential of direct ammonia fuel cells for electricity generation in vehicles, hydrogen refilling stations, and ammonia combustion for power underscores the need for ammonia decomposition under mild conditions. Although progress toward the commercialization of direct ammonia fuel cells is ongoing, in the future, within both distributed and grid power supply systems, a carbon-neutral energy system that combines green ammonia synthesis with ammonia fuel cell technology could become a reality.

In conclusion, combining ML with computational modeling or experiments opens up new possibilities for rapid screening of the catalysts, identifying the performance descriptors, and assisting in catalyst manufacturing. However, further steps are required to couple experimental and theoretical techniques to gain a fundamental understanding, which will inspire researchers to design advanced catalysts for mild-condition ammonia synthesis and decomposition.

Data availability

No primary research results, software or code, have been included and no new data was generated or analyzed as part of this review.

Open Access Article. Published on 04 aprel 2025. Downloaded on 28.01.2026 06:48:11.
This article is licensed under a Creative Commons Attribution-NonCommercial 3.0 Unported Licence.

Conflicts of interest

There are no conflicts to declare.

Acknowledgements

The authors acknowledge funding from the US National Science Foundation (NSF) grant (IIP 1939876). The NSF supported this study (Award numbers: 2315268—the Great Lakes Water Innovation Engine and 2314720).

References

1 M. El-Shafie, S. Kambara, S. P. Katikaneni, S. N. Paglieri and K. Lee, *Int. J. Hydrogen Energy*, 2024, **65**, 126–141.
2 X. Niu, C. Li, X. Li and Y. Zhang, *Heliyon*, 2024, **10**, e25087.
3 Z. Bao, D. Li, Z. Wang, Y. Wen, L. Jin and H. Hu, *Fuel*, 2024, **373**, 132346.
4 F. Schüth, R. Palkovits, R. Schlögl and D. S. Su, *Energy Environ. Sci.*, 2012, **5**, 6278–6289.
5 J. Li, S. Lai, D. Chen, R. Wu, N. Kobayashi, L. Deng and H. Huang, *Front. Energy Res.*, 2021, **9**, 760356.
6 C. Qin, S. Ruan, C. He and L. Zhang, *Colloids Surf., A*, 2024, **691**, 133898.
7 N. Li, C. Zhang, D. Li, W. Jiang and F. Zhou, *Chem. Eng. J.*, 2024, **495**, 153125.
8 M. Ghasemi, J. Choi, S. M. Ghoreishian, Y. S. Huh and H. Ju, *J. Electrochem. Soc.*, 2023, **170**, 074501.
9 N. Zhu, Y. Hong, F. Qian and J. Liang, *Int. J. Hydrogen Energy*, 2024, **59**, 791–807.
10 Z. Bao, D. Li, Y. Wu, L. Jin and H. Hu, *Int. J. Hydrogen Energy*, 2024, **53**, 848–858.
11 S. S. Rathore, S. Biswas, D. Fini, A. P. Kulkarni and S. Giddey, *Int. J. Hydrogen Energy*, 2021, **46**, 35365–35384.
12 G. Glenk and S. Reichelstein, *Nat. Energy*, 2019, **4**, 216–222.
13 Y. Gu, Y. Ma, Z. Long, S. Zhao, Y. Wang and W. Zhang, *Int. J. Hydrogen Energy*, 2021, **46**, 4045–4054.
14 K. Grubel, H. Jeong, C. W. Yoon and T. Autrey, *J. Energy Chem.*, 2020, **41**, 216–224.
15 I. Cabria, *Int. J. Hydrogen Energy*, 2024, **50**, 160–177.
16 Z. Yan, H. Liu, Z. Hao, M. Yu, X. Chen and J. Chen, *Chem. Sci.*, 2020, **11**, 10614–10625.
17 C. Chen, K. Wu, H. Ren, C. Zhou, Y. Luo, L. Lin, C. Au and L. Jiang, *Energy Fuels*, 2021, **35**, 11693–11706.
18 P. Adamou, S. Bellomi, S. Hafeez, E. Harkou, S. M. Al-Salem, A. Villa, N. Dimitratos, G. Manos and A. Constantinou, *Catal. Today*, 2023, **423**, 114022.
19 A. Utsunomiya, A. Okemoto, Y. Nishino, K. Kitagawa, H. Kobayashi, K. Taniya, Y. Ichihashi and S. Nishiyama, *Appl. Catal., B*, 2017, **206**, 378–383.
20 S. Mukherjee, S. V. Devaguptapu, A. Sviripa, C. R. F. Lund and G. Wu, *Appl. Catal., B*, 2018, **226**, 162–181.
21 S. Sun, Q. Jiang, D. Zhao, T. Cao, H. Sha, C. Zhang, H. Song and Z. Da, *Renewable Sustainable Energy Rev.*, 2022, **169**, 112918.
22 S. F. Yin, B. Q. Xu, X. P. Zhou and C. T. Au, *Appl. Catal., A*, 2004, **277**, 1–9.
23 S. M. Ghoreishian, K. Shariati, Y. S. Huh and J. Lauterbach, *Chem. Eng. J.*, 2023, **467**, 143533.
24 T. E. Bell and L. Torrente-Murciano, *Top. Catal.*, 2016, **59**, 1438–1457.
25 Y. Sun, W. Zeng, Y. Yang, Q. Wu and C. Zou, *Chem. Eng. J.*, 2024, **502**, 158043.
26 N. Morlanés, S. P. Katikaneni, S. N. Paglieri, A. Harale, B. Solami, S. M. Sarathy and J. Gascon, *Chem. Eng. J.*, 2021, **408**, 127310.
27 N. Zecher-Freeman, H. Zong, P. Xie and C. Wang, *Curr. Opin. Green Sustainable Chem.*, 2023, **44**, 100860.
28 Z.-W. Wu, X. Li, Y.-H. Qin, L. Deng, C.-W. Wang and X. Jiang, *Int. J. Hydrogen Energy*, 2020, **45**, 15263–15269.
29 K. G. Kirste, K. McAulay, T. E. Bell, D. Stoian, S. Laassiri, A. Daisley, J. S. J. Hargreaves, K. Mathisen and L. Torrente-Murciano, *Appl. Catal., B*, 2021, **280**, 119405.
30 N. Morlanés, S. Sayas, G. Shterk, S. P. Katikaneni, A. Harale, B. Solami and J. Gascon, *Catal. Sci. Technol.*, 2021, **11**, 3014–3024.
31 E. Fu, Y. Qiu, H. Lu, S. Wang, L. Liu, H. Feng, Y. Yang, Z. Wu, Y. Xie, F. Gong and R. Xiao, *Fuel Process. Technol.*, 2021, **221**, 106945.
32 I. Lucentini, A. Casanovas and J. Llorca, *Int. J. Hydrogen Energy*, 2019, **44**, 12693–12707.
33 V. D. B. C. Dasireddy, Š. Hajduk, F. Ruiz-Zepeda, J. Kovač, B. Likozar and Z. C. Orel, *Fuel Process. Technol.*, 2021, **215**, 106752.
34 T. Han, L. Wei, S. Xie, Y. Liu, H. Dai and J. Deng, *Ind. Chem. Mater.*, 2025.
35 Z. Zhao, Z. Liu, M. Li, Y. Yang, L. Deng, Y. Zhao, B. Dou and F. Bin, *Sep. Purif. Technol.*, 2025, **360**, 131144.
36 D. Liang, C. Feng, L. Xu, D. Wang, Y. Liu, X. Li and Z. Wang, *Catal. Sci. Technol.*, 2023, **13**, 3614–3628.
37 J. C. Verschoor, P. E. de Jongh and P. Ngene, *Curr. Opin. Green Sustainable Chem.*, 2024, **50**, 100965.
38 Y. Qiu, E. Fu, F. Gong and R. Xiao, *Int. J. Hydrogen Energy*, 2022, **47**, 5044–5052.
39 G. Li, H. Zhang, X. Yu, Z. Lei, F. Yin and X. He, *Int. J. Hydrogen Energy*, 2022, **47**, 12882–12892.
40 H. Tang, Y. Wang, W. Zhang, Z. Liu, L. Li, W. Han and Y. Li, *J. Solid State Chem.*, 2021, **295**, 121946.
41 G. Li, X. Yu, F. Yin, Z. Lei, H. Zhang and X. He, *Catal. Today*, 2022, **402**, 45–51.
42 M. Pinzón, O. Avilés-García, A. R. de la Osa, A. de Lucas-Consuegra, P. Sánchez and A. Romero, *Sustainable Chem. Pharm.*, 2022, **25**, 100615.
43 A. Jedynak, Z. Kowalczyk, D. Szmigiel, W. Raróg and J. Zieliński, *Appl. Catal., A*, 2002, **237**, 223–226.
44 J. C. Ganley, F. Thomas, E. Seebauer and R. I. Masel, *Catal. Lett.*, 2004, **96**, 117–122.
45 H. Li, L. Guo, J. Qu, X. Fang, Y. Fu, J. Duan, W. Wang and C. Li, *Int. J. Hydrogen Energy*, 2023, **48**, 8985–8996.
46 J. Zhang, M. Comotti, F. Schüth, R. Schlögl and D. S. Su, *Chem. Commun.*, 2007, 1916–1918.
47 L. Li, F. Chen, J. Shao, Y. Dai, J. Ding and Z. Tang, *Int. J. Hydrogen Energy*, 2016, **41**, 21157–21165.
48 M. Feyen, C. Weidenthaler, R. Güttel, K. Schlichte, U. Holle, A.-H. Lu and F. Schüth, *Chem. – Eur. J.*, 2011, **17**, 598–605.
49 H. Zhang, Y. A. Alhamed, A. Al-Zahrani, M. Daous, H. Inokawa, Y. Kojima and L. A. Petrov, *Int. J. Hydrogen Energy*, 2014, **39**, 17573–17582.
50 T. A. Le, Y. Kim, H. W. Kim, S.-U. Lee, J.-R. Kim, T.-W. Kim, Y.-J. Lee and H.-J. Chae, *Appl. Catal., B*, 2021, **285**, 119831.
51 S. Podila, Y. A. Alhamed, A. A. AlZahrani and L. A. Petrov, *Int. J. Hydrogen Energy*, 2015, **40**, 15411–15422.
52 M. Pinzón, A. Romero, A. de Lucas-Consuegra, A. R. de la Osa and P. Sánchez, *Catal. Today*, 2022, **390–391**, 34–47.
53 K. Okura, T. Okanishi, H. Muroyama, T. Matsui and K. Eguchi, *Appl. Catal., A*, 2015, **505**, 77–85.
54 N. Zhu, F. Yang, Y. Hong and J. Liang, *Int. J. Hydrogen Energy*, 2025, **98**, 1243–1261.
55 I. Lucentini, X. Garcia, X. Vendrell and J. Llorca, *Ind. Eng. Chem. Res.*, 2021, **60**, 18560–18611.
56 X. Huang, K. Lei, Y. Mi, W. Fang and X. Li, *Molecules*, 2023, **28**, 5245.
57 S. Mirsadeghi, S. M. Ghoreishian, H. Zandavar, R. Behjatmanesh-Ardakani, E. Naghian, M. Ghoreishian, A. Mehrani, N. Abdolhoseinpoor, M. R. Ganjali, Y. S. Huh and S. M. Pourmortazavi, *J. Environ. Chem. Eng.*, 2023, **11**, 109106.
58 S. M. Ghoreishian, K. S. Ranjith, B. Park, S.-K. Hwang, R. Hosseini, R. Behjatmanesh-Ardakani, S. M. Pourmortazavi, H. U. Lee, B. Son, S. Mirsadeghi, Y.-K. Han and Y. S. Huh, *Chem. Eng. J.*, 2021, **419**, 129530.
59 S. M. Ghoreishian, K. S. Ranjith, M. Ghasemi, B. Park, S.-K. Hwang, N. Irannejad, M. Norouzi, S. Y. Park, R. Behjatmanesh-Ardakani, S. M. Pourmortazavi, S. Mirsadeghi, Y.-K. Han and Y. S. Huh, *Chem. Eng. J.*, 2023, **452**, 139435.
60 H. Martin, C. Ruck, M. Schmidt, S. Sell, S. Beutner, B. Mayer and R. Walsh, *Pure Appl. Chem.*, 1999, **71**, 2253–2262.

 This journal is © The Royal Society of Chemistry 2025

Open Access Article. Published on 04 aprel 2025. Downloaded on 28.01.2026 06:48:11.
This article is licensed under a Creative Commons Attribution-NonCommercial 3.0 Unported Licence.

61 B. G. Petri, R. J. Watts, A. L. Teel, S. G. Huling and R. A. Brown, *In situ chemical oxidation for groundwater remediation*, 2011, pp. 33–88.
62 Z. Yong and T. Ma, *Angew. Chem., Int. Ed.*, 2023, **62**, 202308980.
63 M. Reli, M. Edelmannová, M. Šihor, P. Praus, L. Svoboda, K. K. Mamulová, H. Otoupalíková, L. Čapek, A. Hospodková, L. Obalová and K. Kočí, *Int. J. Hydrogen Energy*, 2015, **40**, 8530–8538.
64 H. Kominami, H. Nishimune, Y. Ohta, Y. Arakawa and T. Inaba, *Appl. Catal., B*, 2012, **111–112**, 297–302.
65 C. Jo, S. Surendran, M.-C. Kim, T.-Y. An, Y. Lim, H. Choi, G. Janani, S. Cyril Jesudass, D. Jun Moon, J. Kim, J. Young Kim, C. Hyuck Choi, M. Kim, J. Kyu Kim and U. Sim, *Chem. Eng. J.*, 2023, **463**, 142314.
66 S. Zhang, Z. He, X. Li, J. Zhang, Q. Zang and S. Wang, *Nanoscale Adv.*, 2020, **2**, 3610–3623.
67 D. Yuan, F. Xie, K. Li, Q. Guan, J. Hou, S. Yang, G. Han, X. San, J. Hao and Y. Li, *Appl. Surf. Sci.*, 2023, **613**, 155973.
68 H. Shi, C. Li, L. Wang, W. Wang, J. Bian and X. Meng, *J. Alloys Compd.*, 2023, **933**, 167815.
69 J. Lin, Y. Wang, W. Tian, H. Zhang, H. Sun and S. Wang, *ACS Catal.*, 2023, **13**, 11711–11722.
70 J. Dzíbelová, S. M. H. Hejazi, V. Šedajová, D. Panáček, P. Jakubec, Z. Baďura, O. Malina, J. Kašlík, J. Filip, Š. Kment, M. Otyepka and R. Zbořil, *Appl. Mater. Today*, 2023, **34**, 101881.
71 S. Zhang, L. Yan, H. Jiang, L. Yang, Y. Zhao, X. Yang, Y. Wang, J. Shen and X. Zhao, *ACS Appl. Mater. Interfaces*, 2022, **14**, 9036–9045.
72 Z. Wang, S. D. Young, B. R. Goldsmith and N. Singh, *J. Catal.*, 2021, **395**, 143–154.
73 Y. Tian, Z. Mao, L. Wang and J. Liang, *Small Struct.*, 2023, **4**, 2200266.
74 R. Sen, S. Das, A. Nath, P. Maharana, P. Kar, F. Verpoort, P. Liang and S. Roy, *Front. Chem.*, 2022, **10**, 861604.
75 A. AlZaabi, F. AlMarzooqi and D. Choi, *Int. J. Hydrogen Energy*, 2024, **94**, 23–52.
76 S. Zisekas, G. Karagiannakis, G. Marnellos and M. Stoukides, *Ionics*, 2002, **8**, 118–122.
77 K. Goshome, T. Yamada, H. Miyaoka, T. Ichikawa and Y. Kojima, *Int. J. Hydrogen Energy*, 2016, **41**, 14529–14534.
78 N. Hanada, S. Hino, T. Ichikawa, H. Suzuki, K. Takai and Y. Kojima, *Chem. Commun.*, 2010, **46**, 7775–7777.
79 D. J. Little, M. R. Smith, III and T. W. Hamann, *Energy Environ. Sci.*, 2015, **8**, 2775–2781.
80 Z. Wu, N. Ambrožová, E. Eftekhari, N. Aravindakshan, W. Wang, Q. Wang, S. Zhang, K. Kočí and Q. Li, *Emergent Mater.*, 2019, **2**, 303–311.
81 N. M. Adli, H. Zhang, S. Mukherjee and G. Wu, *J. Electrochem. Soc.*, 2018, **165**, J3130.
82 J.-J. Zhong, S.-P. Huang, J.-F. Gu, Y. Li, K.-N. Ding, Y.-F. Zhang, W. Lin and W.-K. Chen, *Appl. Surf. Sci.*, 2023, **609**, 155280.
83 J. A. Herron, P. Ferrin and M. Mavrikakis, *J. Phys. Chem. C*, 2015, **119**, 14692–14701.
84 P. Modisha and D. Bessarabov, *Int. J. Electrochem. Sci.*, 2016, **11**, 6627–6635.
85 B.-X. Dong, H. Tian, Y.-C. Wu, F.-Y. Bu, W.-L. Liu, Y.-L. Teng and G.-W. Diao, *Int. J. Hydrogen Energy*, 2016, **41**, 14507–14518.
86 M. Idamakanti, E. B. Ledesma, R. R. Ratnakar, M. P. Harold, V. Balakotaiah and P. Bollini, *ACS Eng. Au*, 2023, **4**, 71–90.
87 Y.-S. Son, K.-H. Kim, K.-J. Kim and J.-C. Kim, *Plasma Chem. Plasma Process.*, 2013, **33**, 617–629.
88 D. Varisli, C. Korkusuz and T. Dogu, *Appl. Catal., B*, 2017, **201**, 370–380.
89 M. Akiyama, K. Aihara, T. Sawaguchi, M. Matsukata and M. Iwamoto, *Int. J. Hydrogen Energy*, 2018, **43**, 14493–14497.
90 P. Peng, J. Su and H. Breunig, *Energy Convers. Manage.*, 2023, **288**, 117166.
91 Z. Wang, H. Zhang, Z. Ye, G. He, C. Liao, J. Deng, G. Lei, G. Zheng, K. Zhang, F. Gou and X. Mao, *Int. J. Hydrogen Energy*, 2024, **49**, 1375–1385.
92 K. H. R. Rouwenhorst, Y. Engelmann, K. van't Veer, R. S. Postma, A. Bogaerts and L. Lefferts, *Green Chem.*, 2020, **22**, 6258–6287.
93 L. Wang, Y. Yi, Y. Zhao, R. Zhang, J. Zhang and H. Guo, *ACS Catal.*, 2015, **5**, 4167–4174.
94 N. Wang, H. O. Otor, G. Rivera-Castro and J. C. Hicks, *ACS Catal.*, 2024, **14**, 6749–6798.
95 J. Moszczyńska, X. Liu and M. Wiśniewski, *Int. J. Mol. Sci.*, 2022, **23**, 9638.
96 S. Shibuya, Y. Sekine and I. Mikami, *Appl. Catal., A*, 2015, **496**, 73–78.
97 M. Reli, N. Ambrožová, M. Šihor, L. Matějová, L. Čapek, L. Obalová, Z. Matěj, A. Kotarba and K. Kočí, *Appl. Catal., B*, 2015, **178**, 108–116.
98 Y.-N. Li, Z.-Y. Chen, S.-J. Bao, M.-Q. Wang, C.-L. Song, S. Pu and D. Long, *Chem. Eng. J.*, 2018, **331**, 383–388.
99 S. Pu, D. Long, M.-Q. Wang, S.-J. Bao, Z. Liu, F. Yang, H. Wang and Y. Zeng, *Mater. Lett.*, 2017, **209**, 56–59.
100 H. Zhang, Q.-Q. Gu, Y.-W. Zhou, S.-Q. Liu, W.-X. Liu, L. Luo and Z.-D. Meng, *Appl. Surf. Sci.*, 2020, **504**, 144065.
101 R. Wang, T. Xie, Z. Sun, T. Pu, W. Li and J.-P. Ao, *RSC Adv.*, 2017, **7**, 51687–51694.
102 W. Guo and H. Liu, *Chem. Res. Chin. Univ.*, 2017, **33**, 129–134.
103 B. Achrai, Y. Zhao, T. Wang, G. Tamir, R. Abbasi, B. P. Setzler, M. Page, Y. Yan and S. Gottesfeld, *J. Electrochem. Soc.*, 2020, **167**, 134518.
104 L. Cunci, C. V. Rao, C. Velez, Y. Ishikawa and C. R. Cabrera, *Electrocatalysis*, 2013, **4**, 61–69.
105 J. C. M. Silva, S. Ntais, É. Teixeira-Neto, E. V. Spinacé, X. Cui, A. O. Neto and E. A. Baranova, *Int. J. Hydrogen Energy*, 2017, **42**, 193–201.
106 N. Sacré, M. Duca, S. Garbarino, R. Imbeault, A. Wang, A. Hadj Youssef, J. Galipaud, G. Hufnagel, A. Ruediger and L. Roue, *ACS Catal.*, 2018, **8**, 2508–2518.
107 L. Wang, Y. Zhao, C. Liu, W. Gong and H. Guo, *Chem. Commun.*, 2013, **49**, 3787–3789.
108 Q. F. Lin, Y. M. Jiang, C. Z. Liu, L. W. Chen, W. J. Zhang, J. Ding and J. G. Li, *Energy Rep.*, 2021, **7**, 4064–4070.
109 M. El-Shafie, S. Kambara and Y. Hayakawa, *J. Energy Inst.*, 2021, **99**, 145–153.
110 J. A. Andersen, K. van't Veer, J. M. Christensen, M. Østberg, A. Bogaerts and A. D. Jensen, *Chem. Eng. Sci.*, 2023, **271**, 118550.
111 Y. Hayakawa, S. Kambara and T. Miura, *Int. J. Hydrogen Energy*, 2020, **45**, 32082–32088.
112 B. Yan, Y. Li, W. Cao, Z. Zeng, P. Liu, Z. Ke and G. Yang, *J. Am. Chem. Soc.*, 2024, **146**, 4864–4871.
113 J. C. McLennan and G. Greenwood, *Proc. R. Soc. London*, 1928, **120**, 283–295.
114 S. Hirabayashi and M. Ichihashi, *Int. J. Mass Spectrom.*, 2016, **407**, 86–91.
115 W. Guo, A. Shafizadeh, H. Shahbeik, S. Rafiee, S. Motamedi, S. A. Ghafarian Nia, M. H. Nadian, F. Li, J. Pan, M. Tabatabaei and M. Aghbashlo, *J. Energy Storage*, 2024, **89**, 111688.
116 E. Soltanmohammadi and N. Hikmet, *J. Data Anal. Inform. Process.*, 2024, **12**, 544–565.
117 E. Soltanmohammadi, A. Dilek and N. Hikmet, *J. Data Anals Inform. Process.*, 2024, **13**, 46–65.
118 D.-N. Vo, J. Hun Chang, S.-H. Hong and C.-H. Lee, *Chem. Eng. J.*, 2023, **475**, 146195.
119 T. Williams, K. McCullough and J. A. Lauterbach, *Chem. Mater.*, 2019, **32**, 157–165.
120 Z.-H. Lyu, J. Fu, T. Tang, J. Zhang and J.-S. Hu, *EnergyChem*, 2023, **5**, 100093.
121 H. Mashhadimoslem, M. Safarzadeh Khosrowshahi, M. Delpisheh, C. Convery, M. Rezakazemi, T. M. Aminabhavi, M. Kamkar and A. Elkamel, *Chem. Eng. J.*, 2023, **474**, 145661.
122 C. Makhloufi and N. Kezibri, *Int. J. Hydrogen Energy*, 2021, **46**, 34777–34787.